



# Leading modes of wind field variability over the western Tibet Plateau

Jingzhi Wang<sup>1</sup> · Xiao-Feng Li<sup>1,2,3</sup> · Shaofeng Liu<sup>1,3</sup> · Ting Liu<sup>4</sup> · Yongjiu Dai<sup>1,3</sup> · Song Yang<sup>1,3</sup> · Hayley J. Fowler<sup>5</sup>

Received: 11 January 2022 / Accepted: 16 May 2022 / Published online: 27 June 2022  
© The Author(s) 2022

## Abstract

Atmospheric circulations bring moisture from above the ocean to the high mountains of the western Tibet Plateau (TP), thus wind variability is of great importance to the water cycle centered on the western TP. This study therefore examines the leading modes of the wind fields over the western TP. We use the multivariate empirical orthogonal function (MV-EOF) analysis method to detect the dominant wind patterns above the western TP. This method extracts the leading modes of combined meridional and zonal wind variability at 200-hPa in the region of 22° N–50° N, 50° E–92° E. We find the first leading mode of the combined zonal and meridional wind field in the annual mean and in most seasons (spring, summer and autumn) over the western TP shows high similarity to the Western Tibetan Vortex (WTV), a large-scale atmospheric vortex-like pattern recently recognized over the western TP. In winter, the WTV, however, is closer to the second leading mode. We estimate the sensitivity of our results by changing the domain of the MV-EOF analysis region surrounding the western. We find the influence of the WTV is less sensitive to analysis location around the western TP. In short, the WTV generally represents the first leading mode of the wind field in most seasons over the western TP. This study augments our knowledge on wind variability over the western TP.

**Keywords** Western Tibet Plateau · Western Tibetan Vortex · MV-EOF · Leading mode · Horizontal wind fields

## 1 Introduction

The western Tibetan Plateau (TP, to the west of ~90° E) is a giant topography standing high in the middle latitudes, facing into the moist Subtropical Westerly Jet (SMJ) which screams across from the Atlantic Ocean, and the humid monsoonal circulations traveling from the Indian Ocean (Barlow et al. 2007; Du et al. 2016; Liu and Yanai 2001; Randel and Park 2006; Yeh et al. 1958). The rivers originating from the western TP supply millions of people in the mid-west and mid-south Asian countries (Lu et al. 2005; Xu et al. 2008). Because the atmospheric circulation is the only medium to bring moisture from above the ocean to the high mountains of the western TP, wind variability is of great importance to the hydrological cycle centered on the western TP (Hren et al. 2009; Tian et al. 2007; Wei et al. 2017).

The earliest interest on wind variability over the western TP may be traced back to the 1950s. Yeh (1950) documented the principal feature as the existence of two belts of maximum westerlies, one flowing around the southern and the other around the northern edge of the TP. Gu (1951) consequently reported that the two belts of westerlies split by the western TP are merged into one strong westerly jet

---

✉ Xiao-Feng Li  
lixf87@mail.sysu.edu.cn

✉ Shaofeng Liu  
liushaof5@mail.sysu.edu.cn

<sup>1</sup> School of Atmospheric Sciences, Sun Yat-sen University, and Southern Marine Science and Engineering Guangdong Laboratory (Zhuhai), Zhuhai, China

<sup>2</sup> State Key Laboratory of Numerical Modeling for Atmospheric Sciences and Geophysical Fluid Dynamics (LASG), Institute of Atmospheric Physics, Chinese Academy of Sciences, Beijing, China

<sup>3</sup> Guangdong Province Key Laboratory for Climate Change and Natural Disaster Studies, Sun Yat-sen University, Zhuhai, China

<sup>4</sup> State Key Laboratory of Satellite Ocean Environment Dynamics, Second Institute of Oceanography, Ministry of Natural Resources, Hangzhou, China

<sup>5</sup> School of Engineering, Newcastle University, Newcastle upon Tyne, UK

at the downstream of the TP, which seriously impacts the East Asian Climates. Recently, increasing interest in wind variability over the western TP has been invoked due to studies relevant to the “Karakoram Anomaly”. The “Karakoram Anomaly” was firstly proposed by Hewitt (2005), and refers to the slowdown of glacier melt over the central part of the western TP, the Karakoram, with global warming, showing a strong contrast to the accelerating glacier melt over the eastern TP and other parts of the world (Hewitt 2005). A couple of recent studies have tried to explain the “Karakoram Anomaly” in view of the wind or circulation variability above the western TP. For example, Yao et al. (2012) proposed that the main cause is probably decreasing (increasing) precipitation in the Himalayas (eastern) Pamir regions, which results from changes in two different atmospheric circulation patterns; that is, the weakening Indian monsoon and strengthened westerlies. Later, a large-scale vortex-like pattern with a deep or quasi-barotropic structure in its year-to-year atmospheric variability, termed the “Karakoram Vortex” (KV) or the “Western Tibetan Vortex” (WTV), was recognized over the western TP (Forsythe et al. 2017; Li et al. 2018; hereafter, collectively cited as FL1718). Forsythe et al. (2017) then proposed that the WTV seriously impacts (Li et al. 2021, 2019) the near surface air temperature over the western TP in summer, the melting season of Karakoram glaciers, which partly explains the “Karakoram Anomaly”. Mölg et al. (2017) then proposed that a southward shift of the upper-tropospheric westerlies contributes significantly to a west–east (cold–warm) dipole in summer near-surface temperature anomalies across High Asia in the core monsoon season (July–September) by using the Global Wave Train Index (CGT) index, which is consistent with the patterns linked to the WTV (FL1718).

Specially, the WTV refers to an anomalous large-scale vortex-like variability with quasi-barotropic structure prevailing over the western TP in all four seasons, spanning 3–4 times the west–east breadth of the Indian Peninsula (FL1718). Its intensity is measured by the Karakoram Zonal Index (KZI) (FL1718): positive (negative) KZI values indicate an anomalous anti-cyclonic (cyclonic) WTV, which are associated with higher (lower) pressure, warmer (cooler) temperature over the mid-lower troposphere (for example, at the 500 hPa level) and anomalous sinking (rising) motions over the central western TP. The WTV provides the dominant driver of circulation variability over the western TP as it can explain over 50% variance of the western TP circulation on multiple levels throughout the troposphere in most seasons except for in winter (Li et al. 2018). The WTV impacts the near surface air temperature over the western TP through both adiabatic heating (Li et al. 2019) and by modulating cloudiness and thus surface net radiation (Li et al. 2021).

To search for major patterns or “dynamic modes” (Wallace 2000) of circulation variability, empirical orthogonal

functions (EOF)/principal component analysis (PCA) and the multivariate EOF (MV-EOF) analysis have been widely used as the key tools (e.g., Barnston and Livezey 1987; Cohen and Saito 2002; Monahan and Adam 1998; Trenberth and Paolino 1981; Wang 1992). Lorenz (1956) firstly applied EOF analysis to the meteorological element field, and found only the first 8 components (of the 64 principal components) can describe 91% of the total variance of the station sea level pressure (SLP) field over the United States. EOFs have been used as a key tool in recognizing teleconnection patterns, such as the Southern Oscillation (SO) (Walker 1928; Kidson 1975), the North Atlantic Oscillation (NAO) (Thompson and Wallace 1998; Thompson and Wallace 2000; Walker 1928; Walker and Bliss 1932) the Northern Annular and Southern Hemisphere Mode (NAM/SAM) (Gong and Wang 1999; Thompson and Wallace 2000; Thompson and Wallace 1998), the Silk Road Pattern (SRP) (Enomoto et al. 2003; Lu et al. 2002; Yu et al. 2009), the Pacific–Japan (PJ) pattern (Kosaka and Nakamura 2010; Kosaka et al. 2011; Li et al. 2014; Nitta 1987; Sun et al. 2010), the Pacific–North American (PNA) (Barnston and Livezey 1987; Feldstein 2000; Wallace and Gutzler 1981), and even the Madden–Julian Oscillation (MJO) (Lau and Chan 1985; Madden and Julian 1971; Maloney and Hartmann 1998; Wang et al. 2014; Wheeler and Hendon 2004). By using MV-EOF analysis, Wang (1992) extracted the vertical structure of ENSO abnormal modes from the combined seven fields (i.e. SST, convection, surface wind field and OLR, etc.) and studied the phase evolution of ENSO. Kim and Ha (2015) documented that the anthropogenic and natural modes were separated well by using the MV-EOF to synthesize the dynamic and thermodynamic factors including precipitation, SST, and convergence of the vertical integrated moisture flux. In short, the MV-EOF method has been widely used to extract dominant modes of combined atmospheric fields (Hui et al. 2013; Jong-Yeon et al. 2010; Kar et al. 2002; Sohn and Tam 2011).

Over High Asia and the entire TP region, Mölg et al. (2017) studied the leading modes of tropospheric variability by separately imposing both the EOF and REOF methods on signal variable fields of geopotential thickness, specific humidity, meridional, and zonal wind, then reported a number of patterns co-varying with the westerlies. However, the western TP has quite different mechanic and thermodynamic features than the eastern TP (e.g., Gu 1951; Wu et al. 2015; Yeh 1950), and the leading modes of multiple wind fields (i.e. the combined zonal and meridional) over the western TP are still unclear. In particular, Li et al. (2018) found that intensity changes of the WTV are significantly correlated with the tropospheric temperature and geopotential height (HGT) over the western TP. According to the covariation of the temporal variability, Li et al. (2018) documented that the WTV can explain more than 50% of temperature and

HGT changes on multiple levels centered at 65° N in all four seasons except for the winter. A relevant question thus arising is whether the WTV is the leading modes of the wind variability over the western TP. Motivated by this, this study applied MV-EOF analysis on the combined meridional and zonal wind field to investigate the leading modes of atmospheric circulation over the western TP.

The remainder of the paper is arranged as follows. Section 2 introduces the data and methods. Section 3 analyzes the leading modes of the combined meridional and zonal wind field over the western TP. Section 4 examines the leading modes of the combined meridional and zonal wind field over neighboring areas surrounding the western TP. Section 5 summarizes the key findings and provides the discussions.

## 2 Data and methods

### 2.1 Data

The monthly mean atmospheric reanalysis data used in this study is the European Centre for Medium-range Weather Forecasts Reanalysis ERA-Interim (De Dee et al. 2011), because it has a good performance over the western TP among a couple of reanalysis datasets (Forsythe et al. 2017) and it is also convenient to be compared with previous studies using the same datasets (FL1718). Its spatial resolution is  $0.75^\circ \times 0.75^\circ$  (latitude and longitude) and it has 26 levels in the vertical direction. We focus on the 1979–2016 period. The variables used include the zonal wind velocity ( $U$ ,  $\text{m s}^{-1}$ ), the meridional wind velocity ( $V$ ,  $\text{m s}^{-1}$ ) and geopotential height (HGT,  $\text{m}^2\text{s}^{-2}$  or gpm).

The Karakoram Zonal Index (KZI) is the intensity index of the WTV, defined as the standardized anomalous zonal wind gradient around the Karakoram (FL1718). In this study, the KZI is calculated according to the method in Li et al. (2018). The seasonal mean is defined as the average of March–April–May (MAM); December–January–February (DJF), and so on. Note that the winter average in year  $n$  is defined as December in year  $n$  and January–February in year  $n + 1$ .

### 2.2 Multi-variable empirical orthogonal function (MV-EOF) analysis method

MV-EOF analysis is employed in this study, which was introduced by Wang (1992). The MV-EOF method is the same as the conventional EOF method, except the MV-EOF decomposes a combined field of two or more variables, while the conventional EOF decomposes only a single variable field. In other words, the MV-EOF is the conventional EOF of combined fields. The MV-EOF method enables a

more efficient compaction of multifield data and extracts dominant patterns in the spatial phase relationships among various meteorological fields of the derived EOF (Wang 1992).

Here, we apply the MV-EOF analysis on the combined meridional and zonal wind anomaly at the 200 hPa level to analyze the main circulation modes in four seasons and for the annual mean. The anomaly is defined as the departure against the climatology that is calculated as the climatological mean in the period of 1979–2016. The MV-EOF is applied at the 200-hPa isobaric level, the same level for which the KZI is defined. The MV-EOF of the combined variable fields is then decomposed into the corresponding time and space functions. The space function is the space type or mode, and the time function is the time coefficient or principal component corresponding to the mode (Wang 1992).

We mainly show results of applying the MV-EOF in the region of  $22^\circ \text{N}$ – $50^\circ \text{N}$ ,  $50^\circ \text{E}$ – $92^\circ \text{E}$  (centered at  $36^\circ \text{N}$ ,  $71^\circ \text{E}$ ), centered on the main body of the WTV. We find the MV-EOF results are relatively stable and don't change dramatically if the analysis region is made slightly bigger or smaller after a series of sensitivity tests, providing that the MV-EOF analysis areas are centered at  $36^\circ \text{N}$ ,  $75^\circ \text{E}$  (central location of the western TP) within the range of  $0^\circ \text{N}$ – $70^\circ \text{N}$  and  $30^\circ \text{E}$ – $120^\circ \text{E}$  (results not shown). Because the horizontal spatial pattern of the WTV is presented at 500 hPa in previous studies as the correlations between the KZI and the circulation fields (FL1718), we hereby also calculate the spatial patterns of the MV-EOF as the correlations between the PCs and the circulation fields at the same level (500 hPa) for better comparison.

For convenience, the spatial pattern of the first (second or third) MV-EOF mode is denoted as the EOF1 (EOF2, EOF3) and its according time series is denoted as the PC1 (PC2 or PC3). The Pearson correlation coefficient between the standardized PC1 (PC2 or PC3) and the KZI is used to quantify the relationship between the EOF1 (EOF2 or EOF3) and the WTV. Then, we compare the circulation patterns associated with the PC1 (PC2 or PC3) to that associated with the KZI. The spatial correlation coefficient is calculated to represent the similarity between the two spatial patterns ( $U$ ,  $V$  and HGT).

North's rule of thumb is used to test the significance of the MV-EOF (North et al. 1982). Student- $t$  test is used to test the significance of the Pearson correlation coefficient and spatial correlation coefficient after considering the efficient number of degrees of freedom ( $N_{edof}$ ) (Li et al. 2013; Zar 1984). The  $N_{edof}$  can be given by the theoretical approximation: 
$$N_{edof} = \frac{N}{1 + 2 \sum_{i=1}^N \frac{N-i}{N} R_{XX}(i) R_{YY}(i)}$$
  $N$  is the number of data points,  $R_{XX}(i)$  and  $R_{YY}(i)$  are the autocorrelations of two sampled time series ( $i = 1, \dots, N$ ) (Li et al. 2013; Zar 1984).

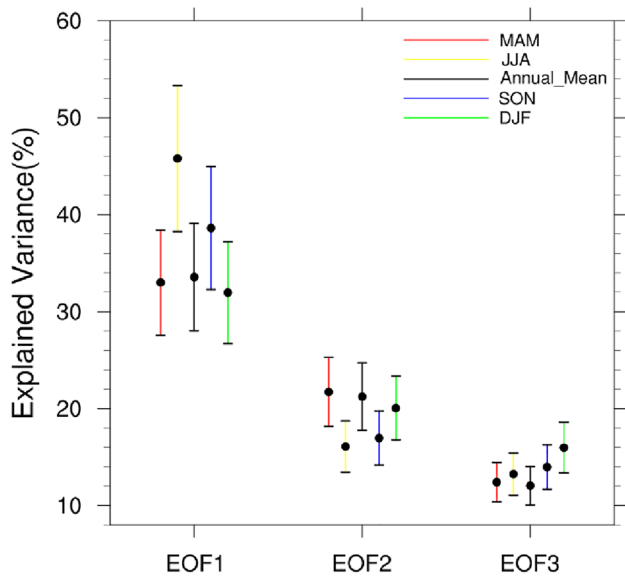


**Fig. 1** Robustness of the MV-EOF analysis (or the EOF analysis of the combined zonal and meridional wind fields). Represented by the explained variance of the first three MV-EOF modes, the error bars are the result from the North et al. (1982) rule. Red, yellow, blue, green and black color is respectively for spring, summer, autumn, winter, and annual mean

**Table 1** Explained variance (%) of the first three leading MV-EOF modes

	Annual mean	MAM	JJA	SON	DJF
EOF1	33.55	32.99	45.78	38.61	31.95
EOF2	21.23	21.73	16.08	16.95	20.05
EOF3	12.04	12.41	13.24	13.98	15.97

### 3 The leading modes of WTV in four seasons and the annual mean

According to North’s rule of thumb, the first three leading MV-EOF modes are significantly separated in all four seasons and the annual mean, demonstrating the uniqueness of these modes. As shown in Fig. 1 and Table 1, the first leading mode in all seasons explain over 30% of total variance, and the explained portion is 33.55% in annual mean. In summer, EOF1 explains 45.78% (nearly half) of the total variance, which is the highest among the four seasons; while, in winter, the explained variance of the EOF1 is the lowest. In all seasons and for the annual mean, the first two leading modes explain over half of the total variance, suggesting the majority of the variability of the wind field over the western TP is represented well by its first two leading MV-EOF modes.

#### 3.1 Annual mean

Comparing the first leading mode (i.e. EOF1) with the WTV, we see significant similarities in spatial patterns between them in the annual mean. To conduct a fairer comparison, the spatial pattern of both the EOF1 and the WTV are represented by the correlation pattern of the PC1 and the KZI with the circulations (horizontal wind and HGT) on the 500 hPa isobaric surface. The horizontal feature of the WTV is usually studied at the 500 hPa level, and it is found to be a pattern in all four seasons and in the annual mean (FL1718). As shown in Fig. 2, the common feature of the atmospheric circulation pattern of the EOF1 and the WTV in the annual mean is: an anticyclonic (cyclonic) wind

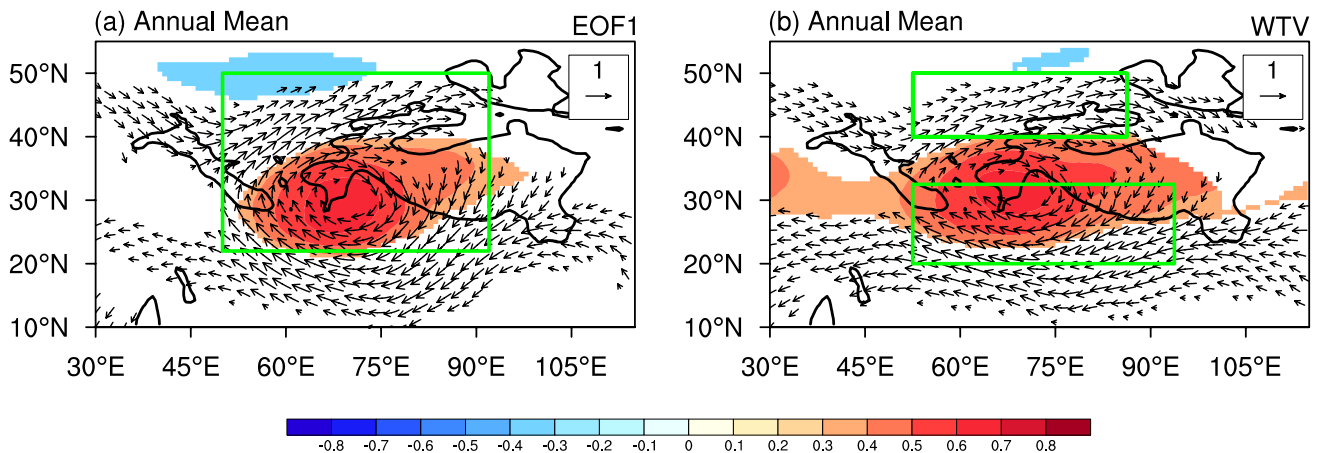


**Fig. 2** Spatial patterns of **a** the EOF1 of the combined horizontal wind field and **b** the WTV for annual mean, which is respectively represented by the correlation coefficients of **a** the standardized PC1 and **b** the KZI with the horizontal wind (vectors) and the geopotential height (color shading) at 500 hpa. Only the correlations significant at 0.05 level after taking account of the efficient numbers of

degrees of freedom are color-shading (Li et al. 2013; Zar 1984); a significant vector denotes either one of its components is significant. The upper right corner is the correlation length scale. The black solid line denotes the topography above 1500 m, the green rectangle in left panel **a** denotes the area selected for MV-EOF, and the green rectangles in right panel **b** are two areas used to calculate the KZI

circulation structure associated with the positive (negative) HGT anomalies centered at the western TP. Visually, there is very limited distinction between the spatial patterns of the EOF1 and the WTV. This can be verified well by the high spatial correlations between them, which reaches 0.91 (also see Table 2). This is also proven well by their highly covariant evolutions in the time series as shown in Fig. 3.

The above result in the annual mean suggests that the WTV generally represents the first leading mode of the wind variability over the western TP. Therefore, we now study the leading modes and their connections with the WTV in all four seasons in the following two sections.

### 3.2 Spring, summer, and autumn

In spring, summer, and autumn, we find the first leading mode (i.e. EOF1) of the wind field over the western TP is highly similar to the WTV.

Comparing the first leading mode (i.e. EOF1) with the WTV in spring, summer, and autumn, we see significant similarities in spatial patterns between them. Shown as Fig. 4a–c vs e–g), the anticyclonic (cyclonic) wind circulation structure associated with the positive (negative) HGT anomalies centered at the western TP are similar between spatial patterns of the EOF1 and the WTV in each season. This is verified well by the high spatial correlations between them shown in Table 2. The spatial correlation of zonal wind, meridional wind and HGT reaches as high as 0.89 except in summer. In summer, the spatial correlations of the EOF1 and the WTV in zonal wind, meridional wind and HGT are relatively lower, but still reach 0.87, 0.77 and 0.71, respectively, significant at the 0.05 level after considering the efficient numbers of degrees of freedom ( $N_{edof}$ ) (Li et al. 2013; Zar 1984).

Accordingly, the temporal variability of the EOF1 and the WTV are also highly correlated to each other in spring, summer, and autumn. The Pearson correlation coefficients between PC1 and KZI respectively reach 0.88, 0.72 and 0.90 in spring, summer, and autumn, all significant at the 0.05

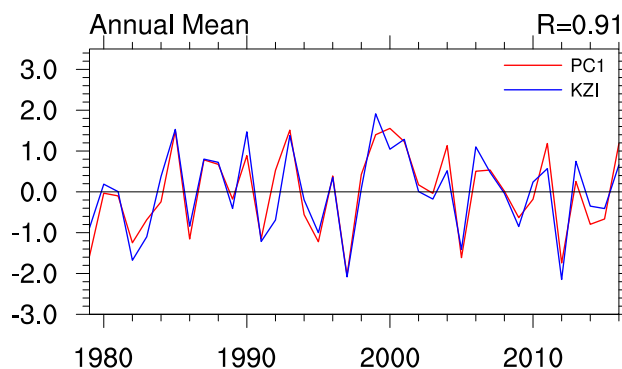


Fig. 3 PC1 (red curve) of the combined horizontal wind field and KZI index (blue curve) in annual mean in the period of the 1979–2016. R represents the correlation coefficient between PC1 and KZI

level after considering the efficient numbers of degrees of freedom. The covariant evolution between the PC1 and the KZI in these seasons are also proved well in Fig. 5a–c. In short, the WTV mainly represents the first leading mode of the wind variability over the western TP in spring, summer, and autumn.

### 3.3 Winter

In winter, however, it is the EOF2 that shows the highest similarity with the WTV among the first three leading modes. As shown in Fig. 4d, the second mode (EOF2) shows a wider horizontal structure in the HGT field, covering the entire Tibetan Plateau, with its associated wind pattern dominated by zonal wind variability. This is basically a similar spatial pattern to the wintertime WTV, shown as their spatial correlation respectively reaches 0.97, 0.82 and 0.93 in the zonal wind, meridional wind, and HGT fields (Table S1). The temporal evolutions of EOF2 and the WTV are highly covariant (Fig. 5d), as evidenced by the Pearson correlation between PC2 and the KZI in winter reaching as high as 0.94. In contrast, wintertime EOF1 and EOF3 show very limited similarity to the WTV; Table S1 and Figure S2 show the

**Table 2** Similarities between the temporal variability and spatial structure of the EOFs of the combined horizontal winds at 200 hPa level and the WTV in the period of 1979–2016

	MAM	JJA	SON	DJF	Annual mean
The Pearson correlation coefficient between PC1 and KZI (DJF, PC2)	0.88	0.72	0.90	0.94	0.91
The spatial correlation coefficient of U between two spatial patterns	0.95	0.87	0.92	0.97	0.97
The spatial correlation coefficient of V between two spatial patterns	0.88	0.77	0.90	0.82	0.92
The spatial correlation coefficient of HGT between two spatial patterns	0.90	0.71	0.92	0.93	0.95

As the horizontal spatial pattern of the WTV was originally given at the 500 hPa level in FL1718, here we thereby calculate all the spatial correlations between the spatial patterns of the WTV and the EOFs on the 500 hPa for better comparisons. The spatial pattern of EOF (WTV) is defined as the Pearson correlation pattern between the PC1/PC2 (KZI) and the horizontal wind (U and V) or HGT field at the 500 hPa. All correlation coefficients significant at 0.05 level after taking account of the efficient numbers of degrees of freedom are color-shaded (Li et al. 2013; Zar 1984)

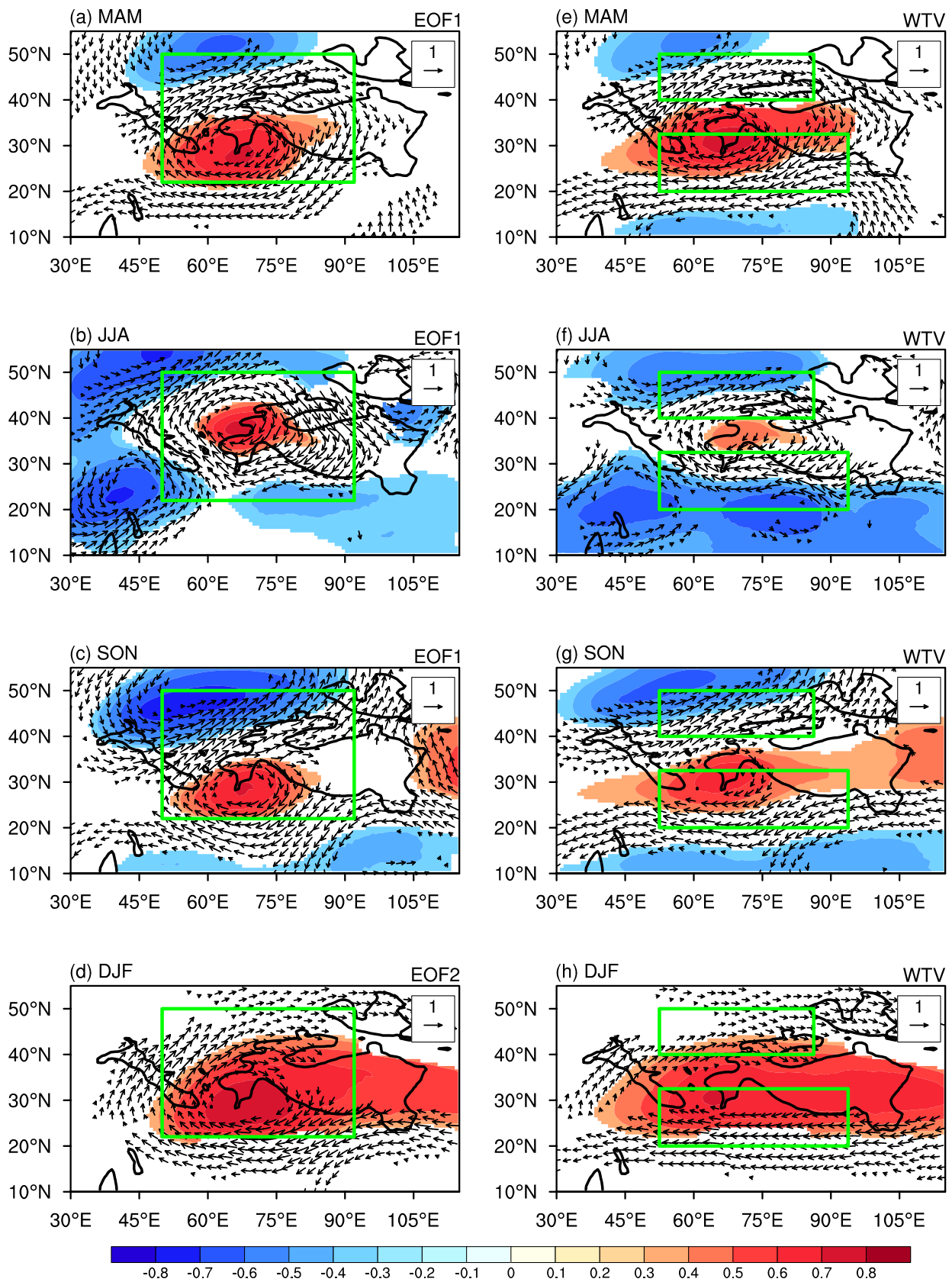


**Fig. 4** Spatial patterns of the EOF1 (left column, **a–c**), EOF2 (left column, **d**) and the WTV (right column, **e–h**) respectively represented by the correlation coefficients of the standardized PC1 (**a–c**), PC2 (**d**), KZI (**e–g**) with the horizontal wind (vectors) and the geopotential height (color shading) at 500 hpa. **a, e** For spring (MAM), **b, f** are for summer (JJA), **c, g** are for autumn (SON), **d, h** are for winter. Only the correlations significant at 0.05 level after taking account of the efficient numbers of degrees of freedom are color-shaded (Li et al. 2013; Zar 1984); a significant vector denotes either one of its components is significant. The upper right corner is the correlation length scale. The black solid line denotes the topography above 1500 m, the green rectangles in left column **a–d** denote the area selected for MV-EOF and in right column **e–h** are two areas used to calculate the KZI

temporal correlations of the KZI with PC1 and PC3 are only 0.25 and 0.03, which are not statistically significant. The spatial similarities of the WTV with EOF1 and EOF3 (Figure S1) are also low, although the U wind field of EOF1 and the V wind field of EOF3 show some similarities. So, the WTV mainly represents EOF2 in winter. This is consistent with Li et al. (2018) who documented that WTV variability explains more variance in spring, summer and autumn but explains less variance in winter.

Although WTV only represents EOF2 in winter, it still shows the best similarity with EOF1 among the first three leading EOFs in the annual mean, spring, summer, and autumn. We thereby conclude that the WTV generally represents the EOF1 of the combined horizontal wind field in the annual mean and in most seasons.

We also note that the seasonal changes of the WTV's spatial pattern are depicted well by the MV-EOF modes. The spatial pattern of the WTV (represented by EOF1) shrinks and reaches its smallest extent in summer, but extends to its biggest east–west size in winter (represented by EOF2). Its central location is at the north of the western TP in summer, but moves to the south of the western TP in other seasons. Besides, the wind field shows as a rounder vortex structure in the spring season, but shows a less round structure in the winter season. In addition, EOF1 explains the highest variance of the wind variability, i.e. 45.78%, in summer, suggesting the summertime WTV dominates the wind variability over the western TP. In contrast, the wintertime WTV explains the least variance of the wind variability among the four seasons, as the explained variance of EOF2 only reaches 21.23%, although it is still a considerable portion.

#### 4 Apply MV-EOF in different areas around western TP

According to the above results, the WTV is represented well by the leading modes of the wind field over the western TP at the box area 22° N–50° N, 50° E–92° E (centered at 36° N, 71° E). The MV-EOF or the EOF is a nonlinear

method (e.g., Storch and Zwiers 2000) independent of the original linear method of recognizing the WTV, i.e. the KZI (FL1817). In other words, the WTV can be recognized by two independent methods over the western TP. A natural hypothesis which then arises is that the WTV is an inherent circulation mode tied up closely with the western TP.

To test the robustness of the hypothesis, we move the checking box area for the regional analysis with its central location slightly out of the central western TP (but is still surrounding the western TP) and recalculate the MV-EOF modes to examine whether the WTV pattern represented by the EOF1 at the central western TP will also move with the checking box area or not. To do this, we chose the area 22° N–50° N, 50° E–92° E (centered at 36° N, 71° E) as the central box area (the same area as in the previous sections, denoted by the green box at the panel with the cross of the horizontal and vertical dashed lines in Fig. 6), then move the box area 5° per test toward four directions surrounding the central box area and re-check the EOF1s. If the WTV pattern represented by the EOF1s in the central western TP is also moving out with the checking box areas, we would conclude that the WTV presented in the previous section is not likely an unique mode, and exists anywhere around and over the TP; otherwise, we suggest that the WTV pattern is an inherent mode physically tied up with the western TP.

#### 4.1 Relatively stable WTV-like patterns along the same latitudes

To begin with, we find the spatial pattern of the EOF1 does not change dramatically when the checking box areas are moved east- or west-ward along a fixed latitude (i.e., the central location of the checking box along 26° N, 31° N, 36° N, 41° N and 46° N) at each column of Fig. 6. For example, the central column in Fig. 6 (column No. 3) is moved along 36° N, the same latitude of the checking area in Fig. 2a. All panels in the central column show an anticyclonic (cyclonic) pattern that is nearly fixed at the same location with little change, except parts of the pattern fade or distort gradually at the far ends as the checking areas are moved away from the western TP. The MV-EOF patterns of these checking areas along 36° N are highly similar to the WTV pattern presented in Fig. 2a, b. In other words, the first leading mode does not change much over the box areas moving 10° west- or east-ward of 71° E along the latitude of 36° N. Similarly, the spatial patterns of the leading mode are also similar to each other when the central location of the checking areas are moved along other latitudes (i.e. 26° N, 31° N, 41° N and 46° N, as shown as other columns in Fig. 6). So, the WTV-like pattern over the western TP represented by the EOF1 is relatively stable without dramatically position shifting during the east- or west-ward moment of the checking areas along the same latitudes.

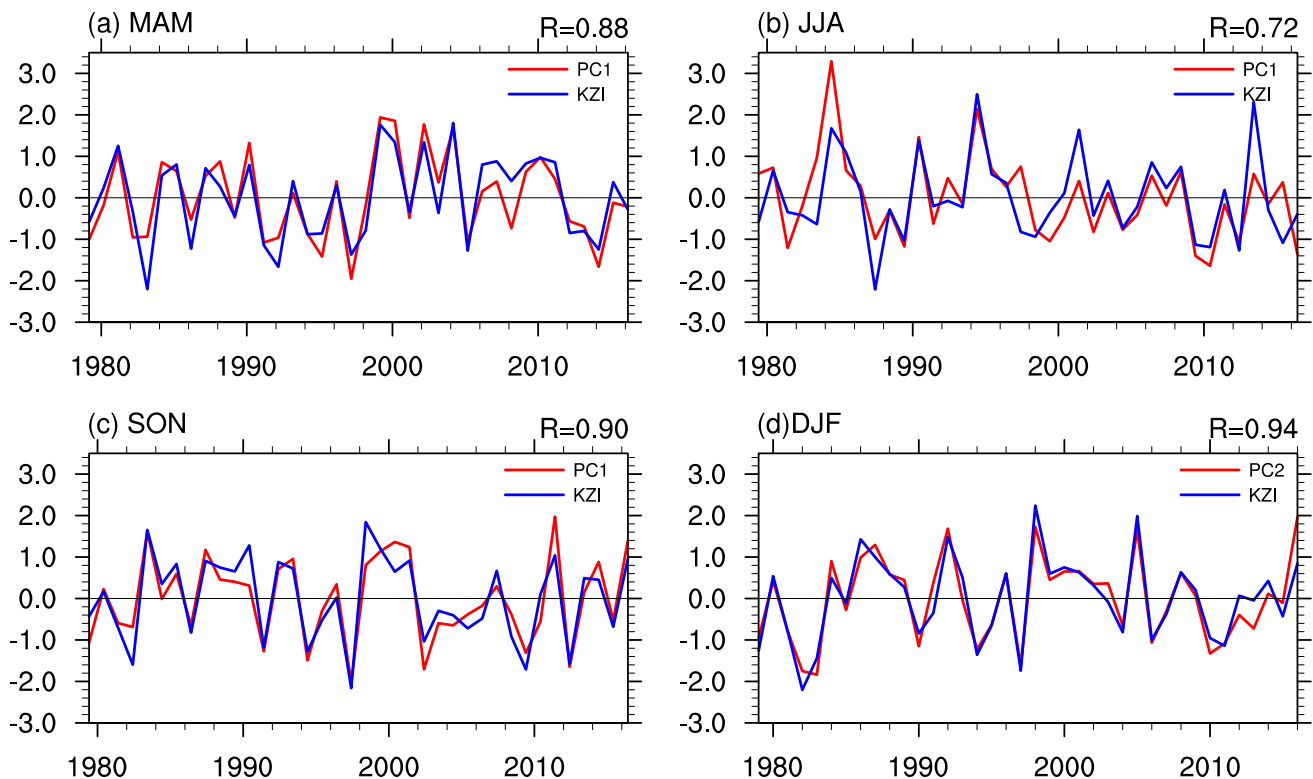


**Fig. 5** PC1 and KZI index **a** MAM, **b** JJA, **c** SON, **d** DJF (PC2) during the period of the 1979–2016. R represents the correlation coefficient between PC1 and KZI

## 4.2 Greater changes of the WTV-like patterns crossing the latitudes

Then, by comparing different columns in Fig. 6, we see the spatial patterns show greater changes between columns to the south (along  $26^{\circ}$  N and  $31^{\circ}$  N) and to the north (along  $41^{\circ}$  N and  $46^{\circ}$  N) of the central box area (along  $36^{\circ}$  N, column No. 3). The spatial patterns of the left two columns (i.e. column No. 1 and 2, respectively along  $26^{\circ}$  N and  $31^{\circ}$  N) in Fig. 6 show more signals from the tropics at around  $10^{\circ}$  N, where there are significant negative correlations between PC1 and the HGT accompanied with significant easterly correlation vectors (between PC1 and wind). Similarly, the spatial patterns of the right two columns (i.e. column no. 4 and 5, respectively along  $41^{\circ}$  N and  $46^{\circ}$  N) in Fig. 6 show more signals from the high latitudes centered at  $55^{\circ}$  N,  $50^{\circ}$  E to the northwest of the western TP. So, the WTV-like pattern represented by EOF1 involves significant tropical (high latitude) signals when the check box area is moved along the latitudes to the south (north) of the central check box area.

This is consistent with previous studies that have already documented that the WTV shows significant correlations with high latitude large-scale atmospheric patterns such as the North Atlantic Oscillation (NAO) and with tropical variability such as the El Niño/Southern Oscillation (ENSO)

(Forsythe et al. 2017), and the WTV is interacting with the westerly jet stream and the South Asian monsoon (FL1718). Therefore, the WTV-like patterns extracted from the checking box areas along latitudes apart from  $36^{\circ}$  N basically reflect more of the connections between the WTV and the neighboring circulations from the tropics and high latitudes.

## 4.3 WTV-like patterns along $36^{\circ}$ N show better similarity to the WTV and better independence to the surroundings

We find the WTV-like patterns along a latitude of  $36^{\circ}$  N show the best temporal and spatial similarity to the WTV among the EOF1s along all latitudes. We quantify their temporal and spatial similarities by calculating temporal and spatial correlations between EOF1 at each checking box area and the WTV in Fig. 7. As shown in Fig. 7a, the temporal correlation between PC1 and the KZI are very high along a latitude of  $36^{\circ}$  N, reaching above 0.9, significant at the 0.05 level after taking account of the efficient numbers of degrees of freedom (Li et al. 2013; Zar 1984). And the temporal correlations drop at latitudes north and south of  $36^{\circ}$  N. A similar feature occurs in the spatial correlations of zonal wind (Fig. 7b), meridional wind (Fig. 7c) and HGT (Fig. 7d). In addition, the temporal and spatial correlations between



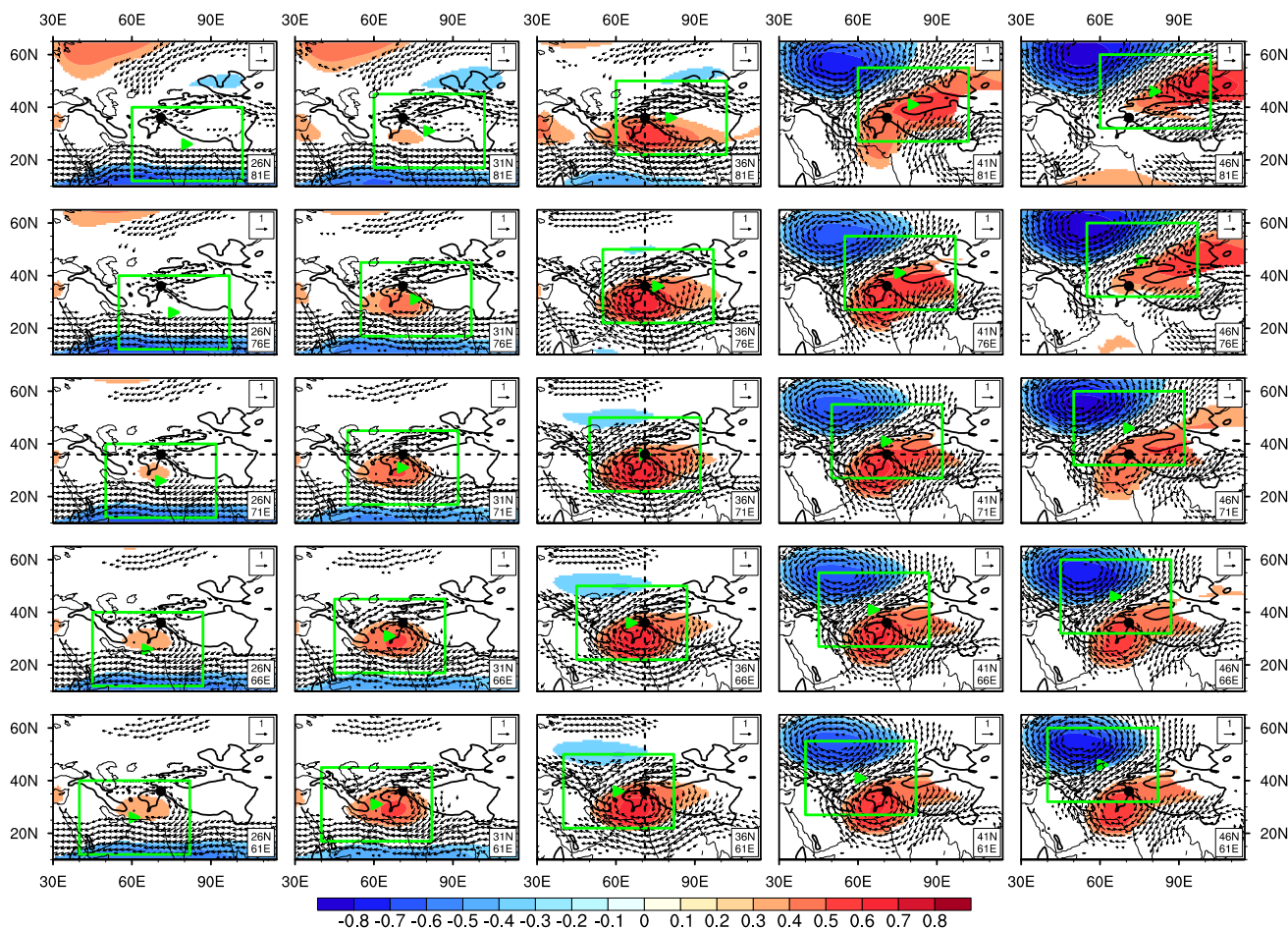


**Fig. 6** Spatial patterns of the first leading mode of the wind field over the western TP and its surrounding areas, represented by correlations of the normalized PC1 with the horizontal wind (vectors) and the HGT (color shading) on 500 hPa level. Green rectangle denotes the MV-EOF decomposing area, whose center location is denoted by the green triangle and the right bottom label at each panel. The area of each green rectangle is as same as 22° N–50° N, 50° E–92° E (center-

ing at 36° N, 71° E, denoted by the black bold dot), except its location is moved 5° or 10° surrounding it. The horizontal and vertical reference lines (black dashed line) are the latitude of 36° N and the longitude of 71° E, respectively, which are crossed at the above central panel. The color shading and vectors are all significant at 0.05 level, same as Fig. 4

EOF1 and the WTV seems to drop faster when the checking areas are moved to the north than to the south except for the meridional wind field. For example, these spatial and temporal correlations drop dramatically when the latitude exceeds 41° N in Fig. 7a, b, d. This seems reasonable as the check box areas along 36° N have the shortest latitudinal distance to the central checking box area.

Besides, it should be noted that the WTV-like patterns represented by the EOF1 of the combined horizontal wind fields along the latitude of 36° N show more independence to the tropical and the high latitudinal signals. As shown as the central column in Fig. 6, when the checking box area is moved eastward or westward along the latitude of 36° N, the spatial patterns of EOF1s involve much fewer significant signals from either the high-latitudes or the tropics than the EOF1s of the checking box areas at the same longitudes

along other latitudes. It suggests the existence of the WTV depends little on the existence of or the impacts from the neighboring tropical or high latitudinal circulations.

In short, the WTV-like patterns found using the MV-EOF method along the latitude of 36° N show better similarity to the WTV, which is also more independent to the neighboring tropical and high latitude circulation variabilities.

#### 4.4 The WTV is tied up in location with the western TP

When the same checking box area is moved 5° per step toward four directions surrounding the central western TP, the horizontal wind data in the MV-EOF analysis changes per step. It is thereby reasonable for us to see that the WTV-like pattern represented by EOF1 changes a bit, as

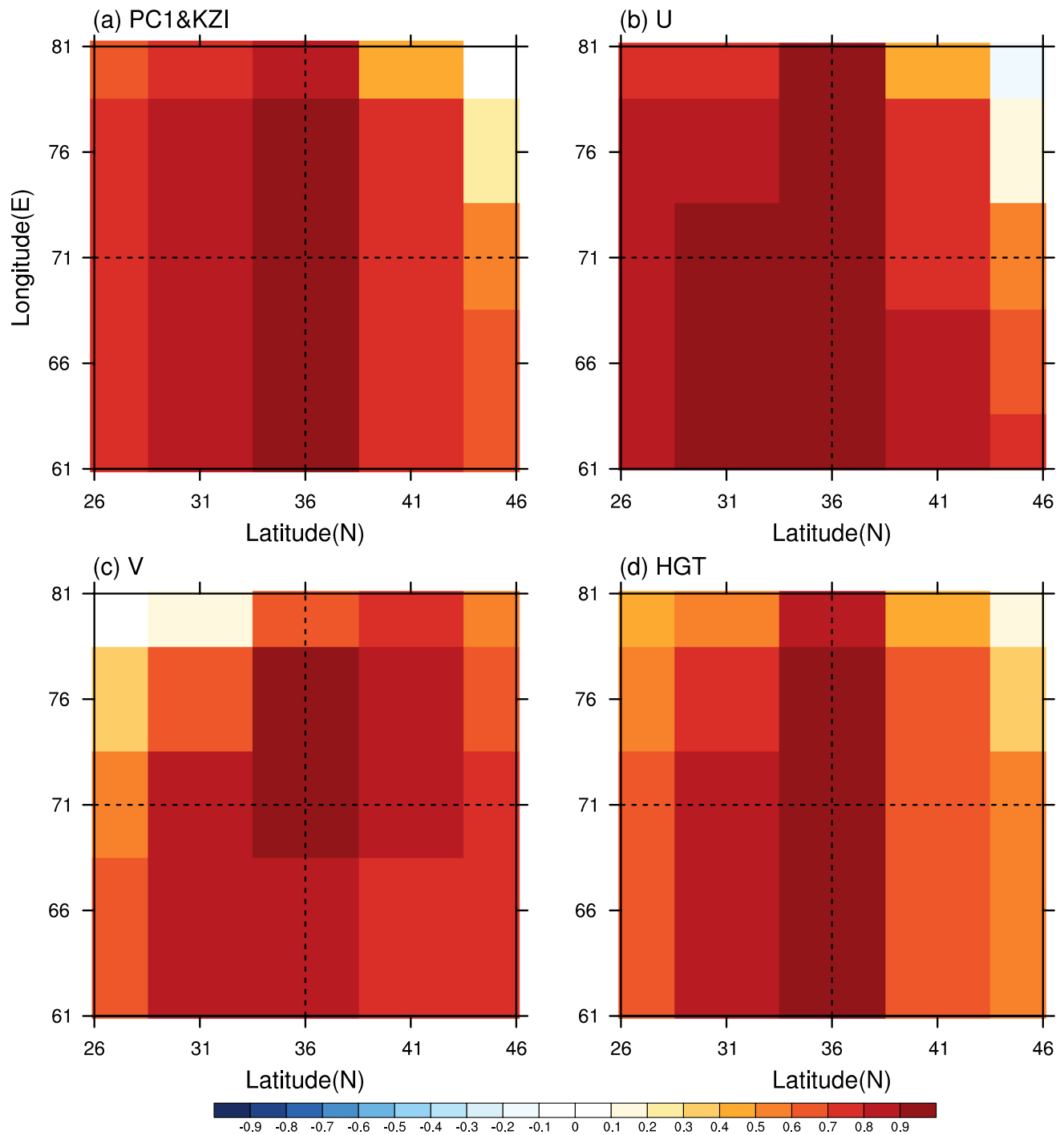


**Fig. 7** The raster of similarity between the first leading MV-EOF mode with the WTV at each checking box area in annual mean presented in Fig. 6. **a** The temporal correlation between the PC1 and the KZI, **b–d** spatial correlations between the **b** zonal wind, **c** meridional wind and **d** HGT of the EOF1 pattern with the WTV pattern. The

abscissa (vertical) axis denotes the latitudes (longitudes) of the central location of the checking box area. Color bar denotes the scale of correlation coefficients. The horizontal and vertical black reference lines (black dashed line) are the latitude of 36° N and the longitude of 71° E, respectively

shown in Fig. 6. As presented in the previous sections, the change is greater when the checking box area is moved latitudinally rather than longitudinally.

However, we emphasize that nearly all the vortex-like patterns over the western TP found by the leading MV-EOF modes in Fig. 6 show similar position and pattern to the

WTV. In addition, although the EOF or the MV-EOF analysis is supposed to be impacted by shape and sizes of the analysis area (e.g., von Storch and Zwiers 1999), we still find the WTV-like pattern changes little (figures not shown) if we choose a box area slightly bigger or smaller than the currently used central box area of 22° N–50° N, 50° E–92° E, providing that the center of the checking box area is located at the central area of the western TP. Therefore, we conclude that the WTV pattern is a circulation mode physically tied up with the topography of the western TP, which can be recognized by either the KZI or the MV-EOF of the combined horizontal wind fields over the western TP.

## 5 Conclusions and discussions

This study explores the major modes of the horizontal wind field over the western TP by using the MV-EOF method. We find the first leading mode in the annual mean and in most seasons are highly like the WTV, a large-scale deep circulation pattern recognized by FL1718. In winter, it is the second leading mode of the combined horizontal wind field that is very similar to the WTV. The WTV was originally recognized (FL1718) by using a standardized zonal wind shear index, namely the KZI (Forsythe et al. 2017); positive (negative) KZI values indicate an anomalous anti-cyclonic (cyclonic) circulation above the western TP. The leading modes of the horizontal wind field over the western TP presented in this study show limited differences with the WTV in both their temporal variability and spatial structure. Here, we thereby conclude that the WTV represents the leading mode of the horizontal wind field over the western TP in most seasons and in the annual mean. This is consistent with the previous study of Li et al. (2018), which analyzed the temporal variabilities of the WTV and meridionally-averaged circulations over the western TP, and documented that the WTV can explain over half of the variability in near surface air temperature (500 hPa) and upper-troposphere (250 hPa) HGT over the WTP in most seasons and in the annual mean, but explains less variance in winter season.

Apart from the MV-EOF of the combined horizontal wind fields, we have also applied conventional EOF to single meteorological variables at the same box checking area, including the zonal wind (U), meridional wind (V), geopotential height (HGT). We find the EOF modes of V or HGT generally show very low spatial and temporal similarities to the WTV (figures not shown). In contrast, the EOF1 of the U shows very high similarity to the WTV in both temporal and spatial variability in all seasons and in the annual mean, as shown in Figure S4–S7 and Table S2. But, the first two EOFs of U in winter do not pass the significance test according to North's rule of thumb (North et al. 1982). Therefore, the leading mode of the conventional EOF of

the zonal wind in most seasons and in the annual mean also represents the WTV except for in winter, and there is no significant EOF mode of U similar to the WTV in winter. It seems that the WTV represents more the zonal wind variability than the meridional wind variability over the western TP in most seasons and in the annual mean.

Moreover, we find the WTV pattern is an inherent mode tied up closely with the western TP. This is mainly supported by two proofs: (1) the identification of the WTV over the western TP is independent of the choice of the methods, both the KZI (the zonal wind gradient index) and the MV-EOFs of the combined horizontal wind fields over the western TP can recognize the WTV; (2) For the MV-EOF methods, no matter if we choose a box area slightly bigger or smaller than the currently used central box area of 22° N–50° N, 50° E–92° E, or move the checking box area out towards four directions over the surrounding areas of the western TP, we can still obtain WTV-like patterns with relatively fixed location and structure, although the features of the WTV-like patterns fade or distort against the WTV with an increase in distance between the check box area and the central western TP.

We notice that EOF1 in summer explains nearly half of the total variance of the wind field, the explained variance reaches 45.78%, which is much higher than the leading modes in other seasons and in the annual mean. It suggests the wind variability of the western TP in summer is more concentrated on EOF1. However, the similarity between the first leading mode of the wind field and the WTV represented by the KZI in summer is relatively lower than in other seasons and in the annual mean. Because the summertime PC1 represents a stronger anticyclonic (cyclonic) structure than does the KZI (Fig. 4b vs f), two relevant questions arise: what causes the KZI to capture less anticyclonic (cyclonic) wind variability in summer than in other seasons over the western TP? What causes the wind variability of the western TP in summer to be more concentrated on EOF1? These deserve further investigation but are out of the scope of this study.

**Supplementary Information** The online version contains supplementary material available at <https://doi.org/10.1007/s00382-022-06358-2>.

**Acknowledgements** This study is funded by the Natural Science Foundation of China (Grants 42088101, 42175026, 41875128), the Guangdong Province Key Laboratory for Climate Change and Natural Disaster Studies (Grant 2020B1212060025), and the Innovation Group Project of Southern Marine Science and Engineering Guangdong Laboratory (Zhuhai) (311021009 and 311021001). The ERA Interim data are publicly available from <https://www.ecmwf.int/en/forecasts/datasets/reanalysis-datasets/era-interim>.

**Funding** Funding was provided by Natural Science Foundation of China (Grants nos. 42088101, 42175026, 41875128), the Guangdong Province Key Laboratory for Climate Change and Natural Disaster

Studies (Grant no. 2020B1212060025), and the Innovation Group Project of Southern Marine Science and Engineering Guangdong Laboratory (Zhuhai) (Grant nos. 311021009 and 311021001).

**Data availability** Enquiries about data availability should be directed to the authors.

## Declarations

**Conflict of interest** The authors have not disclosed any competing interests.

**Open Access** This article is licensed under a Creative Commons Attribution 4.0 International License, which permits use, sharing, adaptation, distribution and reproduction in any medium or format, as long as you give appropriate credit to the original author(s) and the source, provide a link to the Creative Commons licence, and indicate if changes were made. The images or other third party material in this article are included in the article's Creative Commons licence, unless indicated otherwise in a credit line to the material. If material is not included in the article's Creative Commons licence and your intended use is not permitted by statutory regulation or exceeds the permitted use, you will need to obtain permission directly from the copyright holder. To view a copy of this licence, visit <http://creativecommons.org/licenses/by/4.0/>.

## References

- Barlow M, Hoell A, Colby F (2007) Examining the wintertime response to tropical convection over the Indian Ocean by modifying convective heating in a full atmospheric model. *Geophys Res Lett* 34:L19702. <https://doi.org/10.1029/2007GL030043>
- Barnston AG, Livezey RE (1987) Classification, seasonality and persistence of low-frequency atmospheric circulation patterns. *Mon Weather Rev* 115(6):1083–1126. [https://doi.org/10.1175/1520-0493\(1987\)1152.0.CO;2](https://doi.org/10.1175/1520-0493(1987)1152.0.CO;2)
- Cohen J, Saito KJOC (2002) A test for annular modes. *J Clim* 15(17):2537–2546. Retrieved Jun 17, 2022. [https://doi.org/10.1175/1520-0442\(2002\)0152.0.CO;2](https://doi.org/10.1175/1520-0442(2002)0152.0.CO;2)
- De Dee RP, Uppala S, VJQJOTRM Society (2011) The ERA-interim reanalysis: configuration and performance of the data assimilation system. *Q J R Meteorol Soc* 137:553–597. <https://doi.org/10.1002/qj.828>
- Du Y, Li T, Xie Z, Zhu Z (2016) Interannual variability of the Asian subtropical westerly jet in boreal summer and associated with circulation and SST anomalies. *Clim Dyn* 46:2673–2688
- Enomoto T, Hoskins BJ, Matsuda Y (2003) The formation mechanism of the Bonin high in August. *Q J R Meteorol Soc* 129:157–178. <https://doi.org/10.1256/qj.01.211>
- Feldstein SB (2000) The timescale, power spectra, and climate noise properties of teleconnection patterns. *J Clim* 13(24):4430–4440. [https://doi.org/10.1175/1520-0442\(2000\)0132.0.CO;2](https://doi.org/10.1175/1520-0442(2000)0132.0.CO;2)
- Forsythe N, Fowler HJ, Li XF, Blenkinsop S, Pritchard DJNCC (2017) Karakoram temperature and glacial melt driven by regional atmospheric circulation variability. *Nat Clim Change* 7:664–670. <https://doi.org/10.1038/nclimate3361>
- Gong D, Wang S (1999) Definition of Antarctic oscillation index. *Geophys Res Lett* 26:459–462
- Gu Z (1951) Impacts of the Western Tibet Plateau to east Asian climate and its importance. *Acta Meteorol Sin (in Chinese)* 1:43–44
- Hewitt KJMR (2005) The karakoram anomaly? glacier expansion and the 'elevation effect', Karakoram Himalaya. *Mt Res Dev* 25:332–340. [https://doi.org/10.1659/0276-4741\(2005\)025](https://doi.org/10.1659/0276-4741(2005)025)
- Hren MT, Bookhagen B, Blisniuk PM, Booth AL, Chamberlain CPJE, Letters PS (2009)  $\delta^{18}O$  and  $\delta D$  of streamwaters across the Himalaya and Tibetan Plateau: implications for moisture sources and paleoelevation reconstructions. *Earth Planet Sci Lett* 288:20–32. <https://doi.org/10.1016/j.epsl.2009.08.041>
- Hui D, Greatbatch RJ, Park W, Latif M, Semenov VA, Sun XJCD (2013) The variability of the East Asian summer monsoon and its relationship to ENSO in a partially coupled climate model. *Clim Dyn* 42:367–379. <https://doi.org/10.1007/s00382-012-1642-3>
- Jong-Yeon Y et al (2010) Decadal changes in two types of the western North Pacific subtropical high in boreal summer associated with Asian summer monsoon/El Niño-Southern Oscillation connections. *J Geophys Res* 115:D21129. <https://doi.org/10.1029/2009JD013642>
- Kar SC, Sugi M, Sato NJJOTMSOJ (2002) Interannual variability of the Indian Summer Monsoon and internal variability in the JMA global model simulations. *Ser II* 79(2):607–623. <https://doi.org/10.2151/jmsj.79.607>
- Kidson JW (1975) Tropical eigenvector analysis and the southern oscillation. *Mon Weather Rev* 103:187–196
- Kim BH, Ha KJCD (2015) Observed changes of global and western Pacific precipitation associated with global warming SST mode and mega-ENSO SST mode. *Clim Dyn* 45:3067–3075. <https://doi.org/10.1007/s00382-015-2524-2>
- Kosaka Y, Nakamura H (2010) Structure and dynamics of the summertime Pacific–Japan teleconnection pattern. *Q J R Meteorol Soc* 132(619):2009–2030
- Kosaka Y, Xie S-P, Nakamura H (2011) Dynamics of interannual variability in summer precipitation over East Asia. *J Clim* 24(20):5435–5453
- Lau KM, Chan PHJMWR (1985) Aspects of the 40–50 day oscillation during the Northern Winter as inferred from outgoing longwave radiation. *Mon Weather Rev* 113(11):1889–1909. [https://doi.org/10.1175/1520-0493\(1985\)1132.0.CO;2](https://doi.org/10.1175/1520-0493(1985)1132.0.CO;2)
- Li X-F, Yu J, Li Y (2013) Recent summer rainfall increase and surface cooling over Northern Australia since the late 1970s: a response to warming in the tropical Western Pacific. *J Clim* 26:7221–7239
- Li R, Zhou W, Li T (2014) Influences of the Pacific–Japan teleconnection pattern on synoptic-scale variability in the Western North Pacific. *J Clim* 27(1):140–154
- Li X-F, Fowler HJ, Forsythe N, Blenkinsop S, Pritchard D (2018) The Karakoram/Western Tibetan vortex: seasonal and year-to-year variability. *Clim Dyn* 52:3883–3906
- Li X-F, Fowler HJ, Yu J, Forsythe N, Blenkinsop S, Pritchard D (2019) Thermodynamic controls of the Western Tibetan Vortex on Tibetan air temperature. *Clim Dyn* 53:4267–4290
- Li X-F, Yu J, Liu S, Wang J, Wang L (2021) Structure of the Western Tibetan Vortex inconsistent with a thermally-direct circulation. *Clim Dyn*. <https://doi.org/10.1007/s00382-021-06001-6>
- Liu X, Yanai M (2001) Relationship between the Indian monsoon rainfall and the tropospheric temperature over the Eurasian continent. *Q J R Meteorol Soc* 127:909–937. <https://doi.org/10.1002/qj.49712757311>
- Lorenz EN (1956) Empirical orthogonal functions and statistical weather prediction. Technical report, Statistical Forecast Project Report 1, Dept. of Meteor., MIT, 49
- Lu RY, Oh JH, Kim BJTA (2002) A teleconnection pattern in upper-level meridional wind over the North African and Eurasian continent in summer. *Tellus A* 54:44–55. <https://doi.org/10.1034/j.1600-0870.2002.00248.x>
- Lu CX, Yu G, Xie GD, IEEE (2005) Tibetan Plateau serves as a water tower. In: IEEE international geoscience & remote sensing symposium
- Madden RA, Julian PRJJA (1971) Detection of a 40–50 day oscillation in the zonal wind in the tropical Pacific. *J Atmos Sci* 28(5):702–708. [https://doi.org/10.1175/1520-0469\(1971\)0282.0.CO;2](https://doi.org/10.1175/1520-0469(1971)0282.0.CO;2)

- Maloney ED, Hartmann DLJOC (1998) Frictional moisture convergence in a composite life cycle of the Madden–Julian oscillation. *J Clim* 11(9):2387–2403. [https://doi.org/10.1175/1520-0442\(1998\)0112.0.CO;2](https://doi.org/10.1175/1520-0442(1998)0112.0.CO;2)
- Mölg T, Maussion F, Collier E, Chiang J, Scherer D (2017) Prominent midlatitude circulation signature in high Asia's surface climate during monsoon: circulation influences on high Asia. *J Geophys Res Atmos* 122:12,702–12,712. <https://doi.org/10.1002/2017J1D027414>
- Monahan AH, Adam HJOC (2000) Nonlinear principal component analysis by neural networks: theory and application to the Lorenz system. *J Clim* 13:821–835. [https://doi.org/10.1175/1520-0442\(2000\)0132.0.CO;2](https://doi.org/10.1175/1520-0442(2000)0132.0.CO;2)
- Nitta T (1987) Convective activities in the tropical Western Pacific and their impact on the northern hemisphere summer circulation. *J Meteorol Soc Jpn Ser II*
- North GR, Bell TL, Cahalan RF, Moeng FJJMWR (1982) Sampling errors in the estimation of empirical orthogonal functions. *Mon Weather Rev* 110(7):699–706. [https://doi.org/10.1175/1520-0493\(1982\)1102.0.CO;2](https://doi.org/10.1175/1520-0493(1982)1102.0.CO;2)
- Randel WJ, Park M (2006) Deep convective influence on the Asian summer monsoon anticyclone and associated tracer variability observed with atmospheric infrared sounder (AIRS). *J Geophys Res* 111:D12314. <https://doi.org/10.1029/2005JD006490>
- Sohn SJ, Tam CYJOTMSOJ (2011) Leading modes of east asian winter climate variability and their predictability: an assessment of the APCC multi-model ensemble. *J Meteorol Soc Jpn* 89:455–474. <https://doi.org/10.2151/jmsj.2011-504>
- Storch H, Zwiers F (1999) Eigen techniques. In: *Statistical analysis in climate research*. Cambridge University Press, Cambridge, pp 289–292
- Storch HV, Zwiers FW (2000) *Statistical analysis in climate research*. 371–373
- Sun X et al (2010) Two major modes of variability of the East Asian summer monsoon. *Q J R Meteorol Soc* 136:829–841. <https://doi.org/10.1002/qj.635>
- Thompson D, Wallace JMJJOC (2000) Annular modes in the extratropical circulation. Part I: month-to-month variability. *J Clim* 13(5):1000–1016. [https://doi.org/10.1175/1520-0442\(2000\)0132.0.CO;2](https://doi.org/10.1175/1520-0442(2000)0132.0.CO;2)
- Thompson DWJ, Wallace JM (1998) The Arctic Oscillation signature in the wintertime geopotential height and temperature fields. *Geophys Res Lett* 25:1297–1300
- Tian L et al (2007) Stable isotopic variations in west China: a consideration of moisture sources. *J Geophys Res* 112:D10112. <https://doi.org/10.1029/2006JD007718>
- Trenberth KE, Paolino DAJMWR (1981) Characteristic patterns of variability of sea level pressure in the northern hemisphere. *Mon Weather Rev* 109(6):1169–1189. [https://doi.org/10.1175/1520-0493\(1981\)1092.0.CO;2](https://doi.org/10.1175/1520-0493(1981)1092.0.CO;2)
- Walker GT (1928) World weather. *Q J R Meteorol Soc* 54:79–87
- Walker GT, Bliss EW (1932) World weather V. *Mem R Meteorol Soc* 4:53–84
- Wallace JM (2000) North Atlantic Oscillation/annular mode: two paradigms—one phenomenon. *Q J R Meteorol Soc* 126:791–805
- Wallace JM, Gutzler DS (1981) Teleconnections in the geopotential height field during the northern hemisphere winter. *Mon Weather Rev* 109(4):784–812
- Wang W, Hung MP, Weaver SJ, Kumar A, Fu XJCD (2014) MJO prediction in the NCEP climate forecast system version 2. *Clim Dyn* 42:2509–2520. <https://doi.org/10.1007/s00382-013-1806-9>
- Wang B (1992) The vertical structure and development of the ENSO anomaly mode during 1979–2013. *1989*
- Wei W, Zhang R, Wen M, Yang SJJOC (2017) Relationship between the Asian westerly jet stream and summer rainfall over Central Asia and North China: roles of the Indian Monsoon and the South Asian high. *J Clim* 30(2):537–552. <https://doi.org/10.1175/JCLI-D-15-0814.1>
- Wheeler MC, Hendon HHJMWR (2004) An all-season real-time multivariate MJO Index: development of an index for monitoring and prediction 132:1917–1932
- Wu G et al (2015) Tibetan Plateau climate dynamics: recent research progress and outlook. *Natl Sci Rev* 2:100–116
- Xu X, Lu C, Shi X, Gao S (2008) World water tower: an atmospheric perspective. *Geophys Res Lett* 35:L20815. <https://doi.org/10.1029/2008GL035867>
- Yao T et al (2012) Different glacier status with atmospheric circulations in Tibetan Plateau and surroundings. *Nat Clim Change* 2:663–667
- Yeh T-C (1950) The circulation of the high troposphere over China in the winter of 1945–46. *Tellus* 2:173–183
- Yeh T, Shihyen D, Meitsiun Li (1958) The abrupt change of circulation over Northern Hemisphere during June and October. *Acta Meteorol Sin (in Chinese)* 29(4):249–263
- Yu K et al (2009) Analysis on the dynamics of a wave-like teleconnection pattern along the summertime Asian jet based on a reanalysis dataset and climate model simulations. *J Meteorol Soc Jpn Ser II* 87(3):561–580
- Zar JH (1984) *Biostatistical analysis*. Prentice Hall, Hoboken

**Publisher's Note** Springer Nature remains neutral with regard to jurisdictional claims in published maps and institutional affiliations.